Development of a Flying Testbed for Airborne Wind Energy Harvesting

André Filipe da Cunha Pereira
andre.c.pereira@tecnico.ulisboa.pt

Instituto Superio Técnico, Lisboa, Portugal

October 2022

Abstract

With the goal of achieving electricity generation solutions that can serve as a complement or even as an alternative to conventional wind turbines (WT), a new and promising class of wind energy exploration, designated Airborne Wind Energy (AWE), has received increasing attention during the last decade, with no mature technology existing as yet. This work aims to set foundations on the subject and contribute to enhance the deployment of this technology also in Portugal. Accordingly, AWE crosswind systems main options at the operational and architectural level are described and thirteen key-factors of AWE exploration are identified. They are categorized in Technical Design Factors, Operational Factors, Manufacturability, Logistics and Social Acceptability Factors. By using them as criteria for a Multi-Criteria Decision Analysis, via Fuzzy Analytic Network Process, the most suitable AWE crosswind system for two distinct exploration sites - on-shore rural and off-shore - as well as the most relevant factors in that decision were inferred. The results point rigid wing pumping-cycle systems with horizontal take-off as the most suitable solutions for both investigated sites. Also, aerodynamic performance resulted as the most relevant decision factor. Then, relevant for a future AWE implementation, the high-altitude wind resource potential in a region of Portugal was studied, using existing models of the wind speed and power vertical profiles, namely the "Log-Linear Law". The importance of considering atmospheric stability conditions was acknowledged and it was concluded that a rural on-shore exploration of this resource would be more advantageous. For the studied region, maximum sustained wind speed of 18 m/s at a height of 250 m was projected. Finally, in order to consolidate foundations for further studies on AWE in Portugal, a flying experimental testbed was developed, resorting to wind tunnel testing to characterize it aerodynamically and in terms of electricity generation. The resulting prototype consists of a radio-controlled aircraft (maximum aerodynamic efficiency of 8.3) and two on-board electric generators connected in series. Flight testing was also done to simulate a number of flight conditions typical of AWE operation. In a steep pitched flight, a 1.3 W output power was obtained for an airspeed of 18.6 m/s. The prototype shows some limitations, however with clear potential for future optimization.

Keywords: Airborne Wind Energy, Fuzzy Analytic Network Process, High-altitude Wind Resource, Wind Tunnel Testing, Electric On-board Generation.

1. Introduction

In the contemporary times, it is hard to name a day-to-day activity or equipment which does not require electricity at some point. The energy consumption is large and it is expected to keep increasing up to 22% by the end of 2050 [1]. Although this increase embodies a worldwide technological development, it also represents one of the most urgent challenges faced nowadays by humankind, since electricity is produced at its most on the account of fossil fuels. To the date, fossil fuels account for more than 80% of the global primary energy demand [2]. Their combustion is the major driver of global warming and its subsequent negative effects, hence it is urgent to keep investing on renewable energy sources and accelerate the development of the related technologies.

Thereby, Airborne Wind Energy (AWE) appears as an innovative way to explore wind energy. Roughly speaking, AWE systems aim to harvest power from winds at higher altitudes than conventional wind turbines (WT), while replacing their tower and inner part of the blades (which have a relatively low contribution to power generation) by a tether. This connects a flying energy harvesting system to a ground station. This idea represents a substantial smaller material investment per unit of usable power than most other renewable energy sources (90% saving as compared to conventional WT [3]). Furthermore it aims to explore high-altitude winds, which are not only stronger, meaning a larger amount of power is available, but also more consistent in time [4].

The fundamentals of AWE were introduced, in the eighties, by Loyd [5], who showed that one could increase the amount of power harvested from the wind with a tethered wing flying in crosswind, i.e. perpendicular to the wind, through reciprocating patterns such as figures of eight. Since then, different companies/research institutions have investigated several concepts on architectural and operational level, and proposed a number of prototypes, but no technology is mature as yet. Particularly, in Portugal, very little has been done to contribute for this technology development, despite being a country that relies on wind energy to produce around 31% of its electricity [6].

Hence, the present work aims to deliver an initial framework on the subject and contribute to enhance the

deployment of this technology in Portugal, by developing and testing a small-scale prototype. The paper is organized as follows: in section 2, a review on AWE crosswind systems, addressing its physical and operational fundamentals, as well as the types of their main components and subsystems, is given; in section 3, the key-factors for AWE exploration and design choice are presented and described; in section 4, a multi-criteria decision analysis, using these factors, is taken to decide, from nine alternatives, which is the most suitable for an AWE implementation in two distinct locations; in section 5, a study on the high-altitude wind resource potential for a region of Portugal is done; in section 6, the development of an experimental testbed is described and testing results are discussed; and, finally, in section 7, conclusions are stated.

2. Background on AWE Crosswind Systems

2.1. Physical Fundamentals

Flying in crosswind with a velocity $-\overrightarrow{V_c}$, in the sense indicated on fig. 1, larger than the true wind speed, $\overrightarrow{V_w}$ (assumed to be uniform and constant, parallel to the ground plane), maximizes performance [5]. The wing, as well as the tether, "sees" an airflow with an apparent airspeed, $\overrightarrow{V_a} = \overrightarrow{V_w} + \overrightarrow{V_c}$, whose intensity may be substantially larger than V_w. In order to reach a certain altitude and to connect the wing to the ground station, an elevation angle is required, which does not allow a perfect crosswind motion, thus reducing the extractable power. Comparing with non-crosswind generation, the aerodynamic forces are stronger, providing one or two orders of magnitude higher power. The crosswind velocity is typically much larger than $V_w \cos\theta$, hence $V_a \approx V_c$, following that the traction force on the tether F_a is approximately equal to the lift L generated by the wing. For the flying system's drag force D_{FS}, it contributes not only the wing but also and mainly the tether.

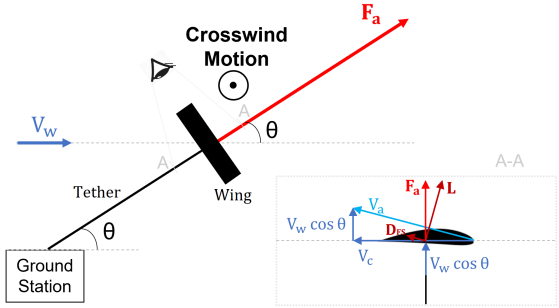

Figure 1: Two-dimensional sketch of the relevant speeds and aerodynamic forces around a wing for wind power generation.

Theoretically, the maximum usable power that any given wing flying in crosswind can extract from a wind field [5] is given by:

$$P_{max} = \frac{2}{27}\,\rho_{air}\,A_{wg}\,(V_w\,\cos\theta)^3\,C_L\left(\frac{C_L}{C_{D_{FS}}}\right)^2 \quad (1)$$

corresponding to an optimal operational apparent wind speed, as follows:

$$V_a^* = \frac{2\,C_L\,\cos\theta}{3\,C_{D_{FS}}}\,V_w \quad (2)$$

where ρ_{air} is the local air density, A_{wg} denotes the wing area, C_L the wing's lift coefficient, and $C_{D_{FS}}$ the flying system's drag coefficient.

There are two general ways of producing electrical energy: on-ground by using the lift-mode concept or on-board the flying unit by using the drag-mode concept.

2.2. On-Ground Generation Systems

In these Systems, electrical energy is produced on the ground station by means of converting mechanical work. As the wing flies with a high crosswind velocity, the generated lift force acts as a traction force to one or more tethers connected to it. The way this force produces motion on the ground generator is the differentiating aspect of the existing configurations. So far, the most propitious type of system is the Pumping-Cycle system. Here, the tethers are then unreeled from an on-ground drum that is linked to an electrical generator. These components are on a fixed ground station.

As its description points out, this kind of system operates in cycles. Each cycle has three consecutive phases: Traction, Transition and Re-Traction [7]. In the first phase, the wing operates in figures of eight at high angle of attack to generate a high traction force, which unreels the tether at a constant speed, producing electricity. In the second phase, the maximum tether length is reached and the wing is positioned to reduce the traction and drag forces to a minimum value. Then, in the last phase, the wing is reeled-in to the original position with minimum energy consumption, so that the cycle may restart. It is also addressed as depowering phase.

2.3. On-Board Generation Systems

In these systems, electric power is produced on-board of the flying wing by onboard wind turbines directly connected to electric generators. In this configuration, the tether remains at constant length, since power is produced not by the traction force acting on the tether but by a drag force generated by the turbines. For optimal power production, the on-board turbines have to increase the flying system's total drag in 50%. Considering N_{rot} turbines/generators, the rotor's optimal area is given by:

$$\frac{A_{rot}}{A_{wg}} = \frac{C_{D_{FS}}}{8\,a\,(1-a)\,N_{rot}} \quad (3)$$

where $A_{rot} = \pi\,D_{rot}^2/4$ is the turbine's rotor area (D_{rot} is its diameter) and a is the rotor's induction factor, which is equal to $1/3$, in ideal conditions (*Betz* limit).

Contrarily to *Lift-mode* systems, *Drag-mode* systems produce electricity continuously, which is then conducted to the ground, via tether. Energy is consumed only for take-off and landing maneuvers.

2.4. Wing Types

The flying wing is arguably the most important component of an AWE system. It must have a high strength-to-weight ratio since it has to withstand large traction loads during climbing and sustaining itself at high altitudes. It must also be controllable in order to be able to operate autonomously. Moreover, it needs to resist to endure mechanical and chemical wearing (e.g. abrasion, corrosion). Many of these characteristics encompass conflicting requirements to achieve an optimal solution. They are, in general, soft or rigid wings, as follows:

2.4.1 Soft Wings

Just like kites, soft wings are usually made of fabric, which makes them very lightweight, compact and crash resistant. On the downside, they have a poor depower behaviour, which is essential for a minimal power consumption in pumping-cycle systems. Another drawback is their lifetime, which is very limited due to the textile involved, so the choice of the material is of extreme importance [8]. These wings are usually controlled from the ground station by steering the tether(s) and/or a bridle system, or from an airborne control unit which steers a bridle system.

The two main types of soft wings are the Leading Edge Inflatable (LEI) wing, which consists of a span-wise inflated tubular frame on the leading edge with an attached single lightweight fabric skin, and the RAM-Air wing, which is a hollow double skin soft wing with larger planform areas. The latter is aerodynamically more efficient as well as easier to control than a LEI kite, although it is heavier and has worse depowering capabilities.

2.4.2 Rigid Wings

Rigid wing systems resemble an aircraft, with its typical actuators for control. They are characterized by having a much superior aerodynamic efficiency than soft wings due to their high aspect ratio, to the usage of profiles with high $^{C_L}/_{C_D}$ and to the fact they almost do not deform [9]. Moreover, due to the materials involved (composite structures), they have a substantial higher durability. However, these advantages come at the price of more expensive manufacturing and of a higher system mass, which limits their performance on low wind speed conditions. Another disadvantage is that, in case of an accident, it is unlikely to recover the wing undamaged.

In AWE, these wings are always used in *Drag-mode* systems, since they are better suited to hold on-board generators. Regarding *Lift-mode* systems rigid wings are claimed to have faster and more efficient traction phases than soft wings.

2.5. Tether

Since its main function is restraining the wing motion, they are designed to withstand high traction forces. In addition, in *Drag-mode* systems, they have to be well insulated to conduct high voltage electricity, while in *Lift-mode* systems, they have to be very resistant to fatigue, due to the cyclic operation. The most negative impact of the tether on power production is its drag contribution [9], which may be estimated from eq. (4), if assumed straight:

$$C_{D,t} = \frac{C_\perp \, l_t \, w_t}{4 \, A_{wg}} \tag{4}$$

where l_t is the tether's length, and w_t and $C_\perp$ are its cross section width and perpendicular drag coefficient. It is larger for *Drag-mode* systems, as tethers are thicker.

2.6. Take-Off and Landing Approaches

The necessary platforms/mechanisms for the take-off/landing maneuvers are the main constituent of the ground station (apart from the generator).

Soft wings usually use a passive approach, meaning the kite is elevated (eg., using a mast) and, when the wind speed is high enough, it takes off automatically. This maneuver may be assisted by on-ground fans.

On the other hand, rigid wings, as they are heavier, consume energy to take-off. There are linear maneuvers which resort to on-board propellers: horizontal take-off (LHT) as a regular aircraft and vertical take-off, as an helicopter (LVT-HO) or with the wing tilted vertically (LVT-VO). There is also the option of a rotational take-off, making use of a rotational arm and the subsequent centrifugal force.

3. Key-Factors for Design Choice

Thirteen factors, categorized in five classes, were identified as determinant for the choice of an AWE system.

3.1. Technical Design Factors, TDF

3.1.1 Aerodynamic Performance, AP

This factor essentially concerns the aerodynamic efficiency of the flying components of an AWE system. For a pumping-cycle system, maximizing the glide ratio $^{C_L}/_{C_{D_{FS}}}$, which appears squared in eq. 1, is critical to achieve maximum power production [10]. It is better to have extremely low drag and moderate lift since, for traction phase, high C_L is required but, for retraction, small wing C_D is essential. Contrarily, for drag-mode systems, maximizing C_L at the account of a substantial increase in C_D seems to lead to higher power production and economical gains [11]. This is accomplished, for example, by using a biplane wing.

3.1.2 Mass-to-Area Ratio, MA

The heavier the system, the larger the elevation angle θ has to be so that the generated lift may balance the flying systems weight. Larger masses also lead to the increase of the minimum wind speed for take-off and operation, which has a strong impact on the potential of power production in a given site. With respect to the flying wing size, larger areas are in general better, since these allow higher power outputs, as seen in eq. (1). Nevertheless, the way area is increased must be well thought, in consideration of the structural mass needed to provide enough stiffness for the required operation. Hence, achieving a small $^m/_{A_w}$ is the goal.

3.1.3 Durability, DU

This factor concerns the period of service life that a given system or subsystem can provide. One can assess the durability of the flying wing based on its materials, and the durability of the tether based on the loads it is is subjected to. The relevance of this factor depends on the site conditions, namely the potential of the site to harm the system and the accessibility for maintenance.

3.1.4 Survivability, SU

This criterion refers to the capacity of the system to remain operational with small or none reparation after a malfunction or accident. This factor can be essentially assessed based on the cost of replacement of the system and on the existence of mechanisms of adaptation to hazardous conditions.

3.2. Operational Factors, OF

3.2.1 Continuity of Power Production, CPP

The capability of supplying electric energy without oscillations implies having a simpler ground station and connection to the grid, since it requires less electrical rectification elements. Although in *Lift-mode* the power is produced discontinuously, the better the depowering

capabilities of the wing, the shorter is the Re-traction phase, hence performing better in CPP.

3.2.2 Controlability, CTR

Controllability of the systems is an extremely important factor for AWE, since it is the main feature to allow for fully automated operation, which is absolutely mandatory for a safe and reliable system posterior commercialization. Rigid wings have a more reliable automation and controllability, as their geometry is always well defined [7]. The actuation surfaces of a rigid wing are more efficient since they are on-board (minimal lag between input and response). The same happens in soft-wing systems using airborne control units, although increasing drag. Furthermore, also concerning controlability of operation, on-board electricity generation is easier to handle than cyclic production.

3.2.3 Take-off/Landing Feasibility, TLF

The take-off/landing systems should be as simpler as possible since that means the associated costs are as lower as possible and the controllers are easier to develop. Regarding rigid wings, a linear vertical take-off/landing maneuver has the smallest complexity, since it requires the smallest ground area and the system has the ability of hovering, although linear horizontal take-off maneuver with a ground acceleration phase and on-board propellers, is established as economically and technically very viable. For soft wings, the use of towers increases the feasibility of a passive approach.

3.3. Manufacturability, M

This class of one single factor concerns the complexity and costs of manufacturing AWE systems. It is clear the need for a feasible and reliable system, which should be obtained with the least possible complexity as well as employing materials with the most availability possible. With respect to the wing, the composite materials and construction processes involved in rigid wings are significantly more costly. In soft wings, although the materials and fabrication processes are generally cheaper, manufacturing challenges occur when scaling-up.

3.4. Logistics, L

This class also corresponds to just one criterion. The logistics complexity and respective costs are mainly linked to the size of the systems and number of components, due to storing and packaging, as well as to the complexity in installation, for which the ground station and associated subsystems such as the take-off/landing platforms are the key players.

3.5. Social Acceptability Factors

3.5.1 Visual Impact, VI

The visual impact is as lower as the airborne system is smaller and its flight path is aesthetic. In terms of size, it is obvious the smaller impact of rigid wing systems. Relatively to the visual appeal of the flight trajectories, the advantages are towards the drag mode operation as it operates continuously in figures of eight. Regarding the ground station, the visual impact is rather low, but distinctions can be done. Ground stations with towers may be considered less visually appealing than the ones with flat take-off platforms.

3.5.2 Noise Impact, NI

The principal source of sound is the generators. For on-ground generation the generator is on the ground station, so if this is built soundproof, the noise effects are negligible This option is not available for on-board generation, hence these systems have the highest noise impact.

3.5.3 Ecological Impact, EI

Another relevant factor for social acceptability is the impact of AWE systems on the local fauna and flora and on the migrating species that may use the airspace of the exploration site. Among the various AWE systems, one may say that the ecological impact of soft wings will be slightly smaller to the one of rigid wings, due to the fact the kites' areas are larger, thus more visible to animals, as well as more likely not to produce a collision. Among rigid wing systems, as on-board generation is louder, it may also reduce the probability of collision.

3.5.4 Safety, SF

The relative safety of these systems can be assessed by considering the risks involved for human life and property in case of a failure and crash of the flying wing. This factor is intrinsically related to the controllability and mass-to-area ratio of the system.

4. Decision of the most suitable AWE system

The question to be answered reads: What is the most appropriate design for a certain exploration site - on-shore rural site, which is an open field location close to an inhabited area, and off-shore site, which is a high-seas location far from populations, but with intense wearing for the systems and with difficult logistics associated?

To answer this question, one applied the Fuzzy Analytic Network Process (FANP) methodology. For sake of brevity, one only presents the method's main steps. For more detail, the reader is referred to [12, 13].

4.1. FANP implementation

4.1.1 Compute a Network

One must identify the decision network nodes, which are the GOAL node, representing the goal of the decision (previous question, which presents two decision scenarios), the criteria nodes on which the analysis will be based (13 key-factors, in section 3) and that can be grouped in clusters (7 key-factor classes, in section 3), and the alternatives nodes on which the decision will act upon. The latter are presented next:

A1: Pumping-cycle system with 1 tether, a rigid monoplane wing (conventional aircraft actuators), and a LHT take-off approach with 1 or 2 on-board propellers;

A2: Same as A1, but with 3 or 4 on-board propellers and a LHT-VO take-off approach;

A3: Pumping-cycle system with 1 tether, a swept rigid wing with on-ground steering mechanisms and a rotational take-off approach;

A4: Pumping-cycle system with 1 tether, a RAM-air wing, an airborne control unit of a bridle system, and a passive approach with elevating mast for take-off;

A5: Pumping-cycle system with 2 tethers, from which the control is done on-ground, and the rest is as A4;

A6: Same as A4, but with a LEI kite and a semi-passive approach for take-off, since it uses, beyond the mast, on-ground fans;

A7: Same as A4, but with a semi-rigid wing in C-shape and an on-ground steering system;
A8: On-board generation system with a rigid monoplane wing (conventional actuators), 8 generators, and a LVT-VO take-off approach;
A9: same as A8, but with a biplane wing.

Then, to complete the decision network, one must identify dependencies between its nodes. In the current decision problem: GOAL depends on (dep.) all criteria, naturally. AP dep. MA, DU and CTR; MA dep. AP; DU dep. GOAL; SU dep. GOAL, MA and CTR; CPP dep. AP and CTR; CTR dep. AP and MA; TLF dep. AP, MA and CTR; M dep. AP, MA and DU; L dep. GOAL, MA and TLF; VI dep. GOAL and MA; NI dep. GOAL; EI dep. GOAL, MA and SU; SF dep. GOAL, MA and CTR; and, finally, alternatives nodes depend on all criteria nodes. Note that, every criteria node also depends on the alternatives nodes, and that the relevancy of the GOAL node varies with the AWE exploration site.

4.1.2 Make Pairwise Comparisons

In order to assess the relative importance of the aforementioned dependencies for each node, pairwise comparison matrices have to be computed, using the Saaty's scale of 1 to 9, where 1 means that the node of the matrix's i^{th} row is as important to the dependant node as the node of the matrix's j^{th} column, and 9 means it is extremely more important [12]. This judgment value is the mean value m^z of a triangular fuzzy number (l^z,m^z,u^z), where l^z and u^z are the lower and upper bounds of the judgment, respectively [13]. Typically, using the Saaty's scale, the l^z and u^z are either 1 or 0.5 higher and lower than the m^z value, respectively, depending on how certain is the analysis. This means that in each comparison, the uncertainty associated to the pairwise judgment subjectivity is quantified by a range of possible "relative importance".

In order to ensure the fuzzy judgments are coherent between themselves, a consistency index (CI) is computed for each comparison matrix. If $CI > 0$, then the judgments performed are consistent, being the consistency as higher as CI is closer to 1 (perfect consistency). If it is null or negative, then the judgments must be reviewed. Since the objective is having the maximum CI, its value is calculated by solving an optimization problem [13]. For a $n \times n$ comparison matrix, the problem is characterized as follows:

$$\begin{cases} \text{maximize} & CI \\ \text{subject to} & \begin{cases} (m_{ij}^z - l_{ij}^z)\, CI\, w_j - w_i + l_{ij}^z\, w_j \leq 0 \\ (u_{ij}^z - m_{ij}^z)\, CI\, w_j + w_i - u_{ij}^z\, w_j \leq 0 \\ \sum_{k=1}^{n} = w_k = 1, \;\; w_k > 0, \;\; k = 1, 2, ..., n \end{cases} \\ \text{for} & i = 1, ..., n-1; \quad j = 2, ..., n; \quad j > i \end{cases}$$

where the vector w is a set of weightings which represents the global relative importance of its dependencies to their dependant.

In the current decision problem, according to the dependencies described earlier, 51 pairwise comparison matrices have to be computed in total for both scenarios. All the comparison matrices are available in [14] alongside the resulting weightings and CI.

Compare dependencies, per cluster, of each criterion node - 5 matrices, available in SMA.2 in [14]: Comparison matrices are only necessary if there is more than one dependency in the same cluster. If it is only one, the weighting of that dependency takes unity, whereas if there is no dependency in the cluster, all the respective weightings take zero.
With respect to AP, MA is strongly more important than DU, not only because of the wing's aspect ratio, but also because the airborne weight influences the required lift force; with respect to CTR, AP is moderately more important than MA; with respect to TLF, both AP and MA are considered to be equally important; and, with respect to EI, MA is considered strongly more important than SU. Concerning M, AP and MA are almost equally important (both are the major factors influencing the materials and fabrication processes involved) and strongly more important than DU.

NOTE:
For the sake of simplicity, in the next cases, one presents criteria or alternatives orderings that represent the basis for the judgments made in the pairwise comparison matrices. If ',' is used, it means the nodes being compared have the same importance (perform equally, if alternatives are being compared) for the node being evaluated, whereas if ';' is used, it means the node on the left is more important (performs better, for alternatives) than the one on the right. The degree of importance may be then obtained, considering the information presented in sections 2 and 3.

Compare criteria with respect to the GOAL node - 6 matrices (3 for each exploration site), available in SMA.1 in [14]. Here, the relative importance is site-dependent, which may only affect the degree of importance, and not the ordering.

In TDF: → AP; MA; DU; SU.
In OF: → CTR; TLF; CPP.
In SAF: → Rural: SF; NI; EI; VI.
→ Off-shore: EI; SF; VI; NI.

Compare alternatives with respect to each criterion - 13 matrices, available in SMA.3 in [14].

AP → A1, A9; A2, A8; A3; A7; A4, A5; A6.
MA → A6; A4, A5; A7; A3; A1; A2; A8, A9.
DU → A8, A9; A3; A1; A2; A7; A5; A4; A6.
SU → A5; A4, A6; A1, A2; A8, A9; A7; A3.
CPP → A8, A9; A1, A2; A3; A7; A6; A4, A5.
CTR → A8, A9; A1, A2; A4, A6; A7; A5; A3.
TLF → A2; A1; A4, A5; A7; A6; A8, A9; A3.
M → A4, A5; A6; A3; A1; A2; A7; A8; A9.
L → A2; A1; A4, A5, A7; A8, A9; A6; A3.
VI → A3; A8, A9; A1, A2; A4, A5, A6, A7.
NI → A4, A5, A7; A3, A6; A1, A2; A8, A9.
EI → A4, A6; A5; A7; A8, A9; A1, A2; A3;
SF → A5; A4, A6; A7; A1, A2; A3; A8, A9.

Compare criteria, per cluster, with respect to each alternative - 27 matrices, available in SMA.4 in [14]. Although different alternatives may have the same ordering, it does not mean the same judgments were given, because the degree of importance may still be different. For that, one assesses the information presented in section 2 and 3.
With respect to TDF:

A1, A2, A8, A9 → AP; DU; MA; SU; / A3 → AP; MA; DU; SU. / A4, A5 → MA; AP; SU; DU. / A6, A7 → AP; MA; DU; SU.

With respect to OF:

A1, A3, A6, A7 → CTR; TLF; CPP. / A2, A4, A5 → TLF; CTR; CPP. / A8, A9, A5 → CPP; CTR; TLF.

With respect to SAF:

A1, A2, A8, A9 → VI; EI, SF; NI. / A3 → VI; NI; EI; SF. / A4, A5, A6, A7 → NI; EI; SF; VI.

4.1.3 Compute Unweighted Supermatrix

The resulting weightings from the comparison matrices are used to compute a supermatrix. Each w set is inserted in the column relative to the dependant, in the rows relative to the dependencies. In the current decision problem, one has a 23×23 unweighted supermatrix for each exploration site, being the first column/row correspondent to the GOAL node; the second to fifth to AP, MA, DU and SU nodes; the sixth to eight to CPP, CTR and TLF nodes; the ninth and tenth to M and L nodes; the eleventh to fourteenth to VI, NI, EI and SF nodes; and the remaining to the alternative nodes by order.

4.1.4 Obtain Normalized Weighted Supermatrix

In this step, the importance of the clusters themselves is addressed. Each group of nodes - the goal group (only 1 element), the criteria clusters and the alternatives group - are matter of comparison. The relevant clusters for comparison are the ones which contain any node that is a dependency of a criterion that is part of the cluster to be evaluated. Hence, the evaluated cluster itself may be part of that comparison.

Having seven network clusters, one has to compute seven comparison matrices for each exploration site (available in SMA.5 in [14]). Accordingly, the same method as before is used. For clusters, where the site leads to differences in the matrices, one presents two orderings, with R for rural and O for off-shore sites.

GOAL:	→	R: TDF; OF; SAF; M; L.
.	→	O: TDF; OF; M; L; SAF.
TDF:	→	R: TDF; OF; Goal, ALT.
.	→	O: TDF; Goal; OG; ALT.
OF:	→	TDF; OF; ALT.
M:	→	TDF; OF.
L:	→	R: ALT; OF; TDF; GOAL.
.	→	O: ALT; GOAL; OF; TDF.
SAF:	→	R:ALT; GOAL; TDF; OF
.	→	O: ALT; TDF; GOAL; OF
ALT:	→	R: TDF; OF; M; SAF; L.
.	→	R: TDF; OF; M; L; SAF.

The resulting weightings then multiply the blocks of columns corresponding to the respective cluster. To normalize the matrix, each column entry is divided by the sum of all entries of that column.

4.1.5 Obtain Limit Supermatrix

To obtain the two limit supermatices, one raises the previous ones to increasing powers until all their columns are equal. The resulting column vector represents the prioritization, from the highest value to the lowest, of both the alternatives and the decision factors. For analysis, one may divide it in two distinct vectors.

4.2. Results and Discussion

For better analysis of the results, one may normalize each vector using the equation $\text{Pref}_{\%,\text{i}} = \frac{x_i - x_{min}}{x_{max} - x_{min}} \times 100$, where x_i are the elements of the vector, and x_{max} and x_{min} are its highest and smallest values. Applying this equation to the column vector resulting from the implementation of FANP, one obtains the results of tables 1 and 2, for the five most suitable alternatives and the five most decisive criteria, for both investigated sites.

Table 1: Alternatives preferences according, via FANP method, for an on-shore rural and an off-shore sites.

	1st	**2nd**	**3rd**	**4th**	**5th**
Rural	A1	A9	A8	A2	A3
$Pref_{\%}$	100	92.03	87.42	86.55	18.77
Off-shore	A1	A2	A9	A8	A4
$Pref_{\%}$	100	85.13	82.65	76.94	29.20

Table 2: Criteria Prioritization, via FANP method, for an on-shore rural and an off-shore sites..

	1st	**2nd**	**3rd**	**4th**	**5th**
	AP	MA	CTR	DU	GOAL
$Pref_{\%}$ - R	100	71.7	34.9	13.6	8.2
$Pref_{\%}$ - O	100	77.0	27.2	15.3	12.3

The results on table 2, show the most relevant criterion for the decision process in both exploration sites is aerodynamic performance, followed by mass-to-area ratio. Regarding the best alternative, the methodology points A1 as the most suitable solution. One also verifies that, in both scenarios, the four best alternatives are the ones with better AP. In the rural exploration site, the difference in preference is smaller than 15%, which indicates all these four alternatives have potential. On the contrary, in the off-shore scenario, A1 is clearly the best solution. Also, here, A2 overcomes the *Drag-mode* systems as the best. This may be explained by an increase of the MA criterion importance, on which A8 and A9 are the worst, as well as a decrease of the CTR criterion importance, on which the *Drag-mode* systems are better than A2. The increase of MA relevancy also leads to an increase of the preference for soft wing systems, which points A4 as the fifth best option instead of A3, as in the rural site.

5. Wind Resource Potential in Portugal

AWE systems aim to explore the wind resource at higher altitudes than conventional WT, which are in average 150 m tall. Furthermore, as shown in [4], there is a significant increase in wind speed up to the first 500 m of the Atmospheric Boundary Layer (ABL). Hence, the typical height range for AWE exploration is from 150 to 500 m, which also coincides with the class of airspace designated for these type of aircrafts (class G).

In order to assess the power production for a given location, one must characterize its wind resource. For most locations there is no wind data available covering the mentioned height range, so it is necessary to use theoretical/semi-empirical models available in the literature. Most AWE related studies apply the classical "Power-law" or Prandtl's Logarithmic Law, which typically present good results for conventional WT, since they are within the ABL's Surface Layer (SL), where

the effects of the mechanical interaction between the airflow and the planet's surface, by action of viscous forces, are dominant. In general, this layer height ranges from 200 m in off-shore locations to 500 m in urban locations (in rural sites is around 300 m). Hence, AWE systems may or may not operate in this region.

Therefore, it is imperative to use models which also take into account the air-surface thermal interaction. Due to a vertical temperature gradient, buoyancy forces arise which induce vertical air motion. This interaction is often addressed as the atmospheric stability. If the environmental lapse rate ($\Gamma = -dT/dh$), i.e. the rate at which temperature decreases with altitude, is equal to the adiabatic lapse rate, which in the troposphere is in average given by $\Gamma_{ad} = 6.5\,\mathrm{K/km}$, the risen air parcel gets in balance with the surroundings and stops rising – one has a neutral atmospheric stratification. If $\Gamma > \Gamma_{ad}$, the risen air parcel, which cools down at the adiabatic lapse rate, stays warmer than its surroundings, hence it continues to rise. This corresponds to an unstable atmospheric stratification, which is typical of diurnal conditions and stimulates turbulence and convective mixing, thus reducing wind shear. Contrarily, if $\Gamma < \Gamma_{ad}$, the risen air parcel becomes colder than its surroundings and sinks, which corresponds to a stable atmospheric stratification, typical of nocturnal conditions. No mixing occurs, unless a source of mechanical energy exists, which leads to larger wind speed gradients.

In order to cope with both surface roughness and atmospheric stability effects on the wind speed vertical profiles, one may use the "log-linear law" [15], as follows:

$$V_w(h) = \frac{v^*}{k}\left[\ln\left(\frac{h}{z_0}\right) - \Psi\left(\frac{h}{L^{Ob}}\right)\right] \qquad (5)$$

where $k = 0.41$ is the von-Kárman constant, z_0 is the surface roughness length, ν^* is the friction velocity, and $\Psi(h/L^{Ob})$ is a correction function, which depends on the Obukhov Length: $L^{Ob} > 0$ indicates stable stratification of the atmosphere; $L^{Ob} < 0$ indicates unstable stratification; and $L^{Ob} = +\infty$ (or very large) indicates neutral stratification. This equation for the vertical wind speed profile is once again valid for the SL, however its applicability is very much related to the stability conditions meaning it can resemble reality for a larger or smaller height range depending on the condition of stability. Typical stability functions are given in table 3:

Table 3: Stability Correction Functions [15].

Atmospheric Stability, Obukhov Length	$\boldsymbol{\psi(h/L^{Ob})}$
Neutral, $L^{Ob} = \infty$	0
Unstable, $L^{Ob} < 0$	$2\ln\left(\frac{1+x}{2}\right) + \ln\left(\frac{1+x^2}{2}\right) - 2\,tan^{-1}(x) + \frac{\pi}{2}\ ,\quad x = \left(1 - 19.3\,\frac{h}{L^{Ob}}\right)^{0.25}$
Stable, $L^{Ob} > 0$	$-\frac{h}{L^{Ob}} - \frac{2}{3}\left(\frac{h}{L^{Ob}} - \frac{5}{0.35}\right)e^{-\frac{0.35\,h}{L^{Ob}}} - \frac{10}{1.05}$

Equation (5) has shown good agreement with experimental results [15], in unstable atmospheric conditions, for a height range up to 500 m for both on- and off-shore locations, which means its applicability surpasses the SL. However, in stability conditions, it was only a good fit up to 200 m, which for on-shore locations is even below the SL height. Therefore, results in these conditions must be seen with caution.

5.1. Wind Speed and Surface Roughness Data

In order to apply equation (5) for a given region, one has to compute the friction velocity. Assuming it is constant, and knowing the wind speed for a reference height, one may compute it using the same equation. Accordingly, the present work is supported on the results of a previous study, where mean wind speed maps representative of the first 50 m of the SL were obtained for three regions of Portugal [16], using NCEP/NCAR reanalysis, covering more than 40 years of climatology observations. The results shown good agreement with measurements at 20 m, hence this was used as a reference height to calculate the friction velocity.

To apply the equation, one also requires the surface roughness lengths for the region of study. This was defined as the region C of [16] - central and coastal area of Portugal. Resorting to the *Global Wind Atlas*, one obtained the corresponding z_0.

5.2. Power Vertical Profiles

In order to estimate wind power maps, one may use the following equation [7]:

$$P_w(h) = \frac{1}{2}\,\frac{p_0}{R_{air}\,T_0}\left(1 - \frac{\Gamma\,h}{T_0}\right)^{\frac{g}{\Gamma\,R}-1} V_w^3(h) \qquad (6)$$

where $p_0 = 101325\,\mathrm{Pa}$ and $T_0 = 288.15\,\mathrm{K}$ are pressure and temperature at the surface in standard atmosphere; $R_{air} = 287.1\,\mathrm{J/kgK}$ is the individual gas constant of air; Γ denotes again the environmental lapse rate; and $g = 9.80665\,\mathrm{m\,s^{-2}}$ is the gravitational acceleration.

By integrating this equation in a height range $\Delta h = h_1 - h_0$, which can be seen as the operational altitude range of a AWE *Drag-mode* system, one obtains the amount of wind power passing through a vertical strip of unit width, ranging from height h_0 to h_1: $P_{w,\Delta h}$.

5.3. Results and Discussion

Using equation 5 and the stability functions of table 3, one computed, for the central region of Portugal, wind speed maps at an height of $h = 250\,\mathrm{m}$, where the equation still provides good estimates in stable atmospheric conditions. They are presented in figures 2 (unstable atmospheric conditions) and 3 (stable atmospheric conditions).

As depicted in the wind speed maps, the minimum wind speeds occur essentially at coastal areas and range from 6.5 to 9 m/s. The correspondent $P_{w,\Delta h}$ ranges from 4 kW/m, in unstable conditions, to 10 kW/m, in stable conditions. Regarding the largest wind speeds, one may observe that these occur more to the interior of the region (eastwards), even though the maximum values also take place in coastal areas (always on-shore). These range from 10.5 to 18 m/s. Regarding the power passing through a vertical strip of unit width, the maximum values vary from 14 to 70 kW/m, which means that there might be an increase of around 400% in available power, from day to night (i.e. from unstable to stable atmospheric conditions).

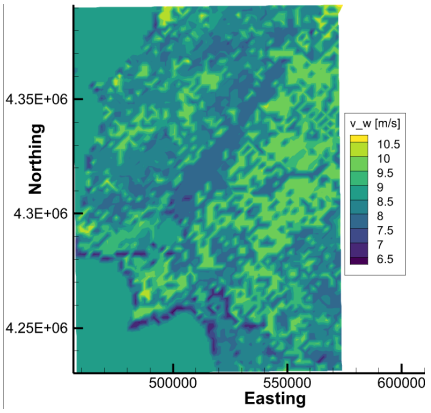

Figure 2: Wind Speed Map in a central region of Portugal, for unstable atmospheric conditions, at $h = 250\,\mathrm{m}$.

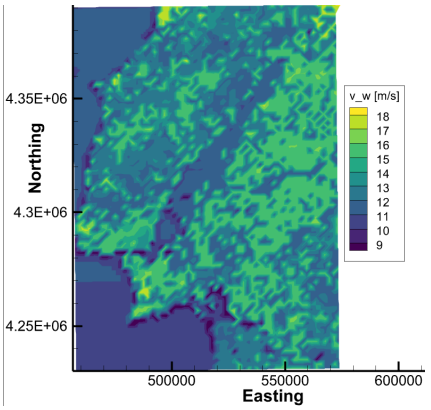

Figure 3: Wind Speed Map in a central region of Portugal, for stable atmospheric conditions, at $h = 250\,\mathrm{m}$.

6. Implementation of an Experimental Testbed

After verifying that harnessing AWE has more potential in an on-shore location and concluding that, for a rural location, the on-board generation alternatives are very suitable, one intends to develop a small-scale flying testbed to a *Drag-mode*.

6.1. Testbed Geometrical Characterization

The basis of the testbed is a radio-controlled aircraft of 780 mm length and 944 mm wing span. The thrust is provided by a 2400 kV brushless motor and a 13 cm diameter 3-blade propeller, in a push configuration. Power is provided by a LiPo battery of 2200 mAh and 11.1 V. The aircraft has a semi-inverted V-tail connected, through two carbon-fiber booms, to a high wing of approximately trapezoidal shape with elliptical tips and area $A_W = 0.14\,\mathrm{m}^2$. Thus, it has an aspect ratio of 6.4. In order to approximate the aircraft of a *Drag-mode* system, two electric brushed generators were mounted on the wing, guaranteeing alignment and lateral symmetry. To harvest wind energy, 3-blade wind turbines of diameter $D_{rot} = 15.2\,\mathrm{cm}$ were connected to the generators through axis adaptors. With these modifications - see figure 4 - the aircraft's "ready-to-fly" mass became $m_{mod} = 0.65\,\mathrm{kg}$.

Figure 4: Developed *Drag-mode* System Flying Testbed.

6.2. Aerodynamic Characterization

In order to aerodynamically characterize the aircraft, one resorted to wind tunnel testing.

6.2.1 Wind Tunnel

The tests were performed in an open-return low-speed wind tunnel with an open section of area $A_{ts} = l_{ts} \times h_{ts} = 1.35 \times 0.8\,\mathrm{m}^2$. The maximum airflow speed at the test section is about 10 m/s with the fan operating at 100%. There, the model is mounted on a Shenck scale with its CG aligned with the support. The scale has 6 measurement cells that allow to determine three forces ($\mathrm{F_{x,y,z}}$) and three moments ($\mathrm{M_{x,y,z}}$). Before each test, a calibration of the scale is automatically done to remove the contribution of the model's weight in the forces and moments measured. It also allows the variation of the angle of attack α of $\pm 30^o$. All measurements taken were within the scale limits. In addition, measurements of the dynamic pressure (p_{din}), in $\mathrm{mmH_2O}$, and temperature (T), in $^{\circ}\mathrm{C}$ are also provided.

6.2.2 Testing Procedures

To analyse both the original and modified aircraft, one performed a test with the fan at 100% power, covering an angle of attack range of $[-16^o, 26^o]$ with a 2^o step. In each iteration, i.e. for each angle of attack, ten measurements were taken with an integration time of 10 s to calculate a mean value. In addition, in order to eliminate the contribution of the model support to the force in x-direction ($F_x^{\text{no\_model}}$) in the post-processing results phase, one also performed a test in the same conditions but without the aircraft mounted and, evidently, without varying the angle of attack. All the tests were performed with Reynolds Numbers differing by less than 1%.

From the measurements obtained for each angle of attack, one determined the lift (C_L) and drag (C_D) coefficients as well as the pitch moment coefficient (C_{My}). At this stage, one decided not to study lateral aerodynamics, given that all the modifications introduced were longitudinally made and keep lateral symmetry so, in that sense, the aircraft should behave in the same way as the original. Furthermore, aerodynamic corrections on the coefficients were performed according to [17], and an uncertainty analysis was included.

6.2.3 Results and Discussion

In the AWE framework, the most interesting results are the lift coefficient and the aerodynamic efficiency, which are presented in figures 5 and 6, respectively.

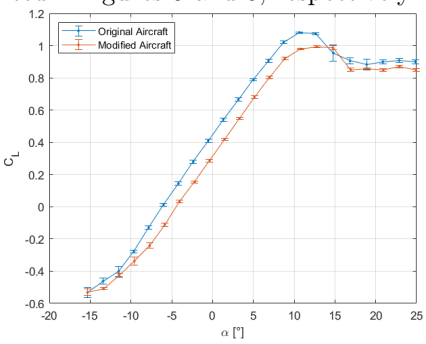

Figure 5: $C_L(\alpha)$ for the original / modified aircrafts.

First of all, the curves on figure 5 reflect little uncertainty in the measurements. Analysing the impact that the modifications on the aircraft's wing brought to the generation of lift, one verifies that these almost did

not affect the rate of C_L with α. However, there was a decrease in C_L values for the whole α range. The maximum lift coefficient became approximately equal to 1 at $\alpha = 13^o$, which represents a 9% decrease. Finally, one also verifies the aircraft has a smooth stall behaviour.

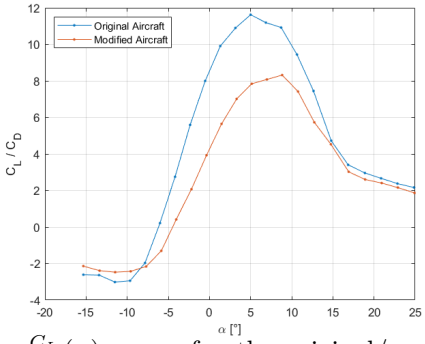

Figure 6: $\frac{C_L}{C_D}(\alpha)$ curve for the original/modified aircrafts.

As depicted in figure 6, the original aircraft's maximum aerodynamic efficiency was about 11.6 at an angle of attack of 5^o. After the modifications, this was reduced to 8.3 at an angle of attack of approximately 9^o, which corresponds to a loss of almost 30%. This was expected due to the reduction of lift and increase in drag brought by the generator-wing interfaces.

6.3. Obtaining Electric Power On-board

In order to assess if and how much power can be harvested with this setup, the electrical efficiency of the generators is estimated, and a simple circuit is specified.

6.3.1 Determining the Generator Efficiency

Concerning electrical efficiency, it is well known that, in general, the efficiency of a machine working as a generator is greater than when working as a motor. Hence, one may determine the motor's efficiency, which is a relatively simple process, and assume that the generator's efficiency is equal or greater than it. The motor's electrical efficiency is obtained by the ratio between the mechanical output power (torque multiplied by rotational speed) and the electrical input power. Since the output torque (Q_M), as well as the input current (I_{in}) and voltage (U_{in}) are linearly related to the motor's rotational speed (n_M), it is necessary to test two operational states.

Providing a voltage of approximately 8.5 V to the motor, measurements of the aforementioned mentioned quantities were taken, for a free-rotation operational state, where the output torque is assumed null, and a mechanical stall operational state, where, in turn, the rotational speed is null. The normalized characteristic curves are presented in figure 7.

Firstly, one observes that, despite being theoretically equal, the motors have different characteristics. Regarding the motor efficiencies, one verifies that one motor has a maximum of approximately 20% achieved at $n_M = 5400$ RPM, whereas the other has a maximum of 30% at $n_M = 6800$ RPM. These efficiencies are particularly low, which may be justified by their small size, by their weariness (these motors are not new) and most likely by a dynamic unbalance between the generator's axis and the turbine adaptor - the small scale of the motors did not allow a perfect alignment. In fact, this unbalance is visible and it is slightly larger in the motor which has lower efficiency. Consequently, it causes vibrations which dissipate energy.

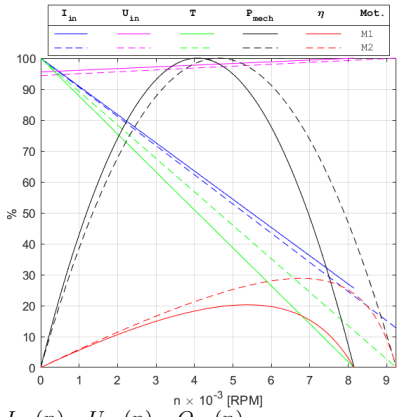

Figure 7: $\frac{I_{in}(n)}{I_{in}^{max}}$, $\frac{U_{in}(n)}{U_{in}^{max}}$, $\frac{Q_M(n)}{Q_M^{max}}$, P_{mech} and η_{elec} curves of the motors used.

6.3.2 Specify the Electrical Circuit

A closed circuit for power production is specified. It is composed by the generators, connected in series or in parallel, and by a load resistance which dissipates the generated power through heat. Using the wind tunnel to simulate a wind flow from which the generators would produce electricity, the two types of connections were tested, covering a resistance range from 5 Ω up to 120 Ω. By measuring the output voltage and by applying Ohm's law, one determined the output power. The resulting curves are showcased in figure 8.

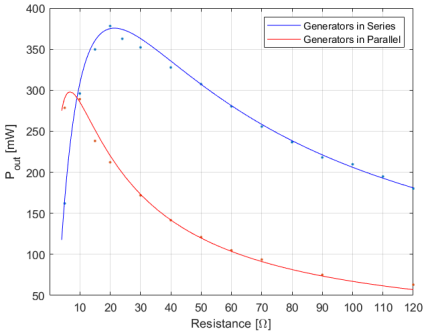

Figure 8: Variation of the output power with the circuit resistance, with the generators connected in series and in parallel.

The maximum output power was obtained, for each configuration, with different resistances, as expected. However, contrarily to the expectations, the maximum values were different. In fact, with the generators in series, the maximum output power was about 375 mW, obtained with a resistance of $R = 20\,\Omega$, whereas with the generators connected in parallel, the maximum was about 300 mW with a resistance of $R = 5\,\Omega$.

As seen, the motor/generator efficiencies are different, which means the output voltages are also different (they operate in the same airflow conditions). Hence, in a parallel connection, since the two generators must have the same output voltage, an electrical flow will pass from one to the other for equalization, which reduces the amount of electricity that flows to the load resistance, which, in turn, reduces the output power.

From this test, one specifies the electrical circuit as the two generators connected in series with a load resistance of $R = 20\,\Omega$.

6.4. Flight Testing

Finally, in order to further understand the potential

of on-board power generation with the developed prototype, one also resorted to flight testing, which allowed to subject the testbed to a realistic scenario of operation, namely to turbulent airflows with larger velocities as well as time and space variability. Although the flight operation is not AWE alike, since there is no tether connected, one may use some of the tested flight conditions to simulate AWE harvesting, namely pitching flight as well as turns - as they take part of a figure eight path.

Thereby, with a multimeter on-board, one performed a number of flight conditions, and recorded, with an on-board camera, the output current and voltage values measured on-board. Since the flight was also recorded from ground, the videos had a correspondence that was used to identify which flight conditions belong the generated output powers. In particular, for a turning flight condition, an output power of 0.814 W at an estimated airspeed of 14.4 m/s was obtained, while for a steep pitched flight, a 1.3 W power for a 18.6 m/s airspeed was the outcome. These tests show that potential for further developments exist.

7. Conclusions

The main outcome of the present work was settling foundations for further studies on Airborne Wind Energy exploration. A review on the physical and operational fundamentals of the different AWE systems and subsystems allowed the identification of thirteen key-factors for AWE design choice. In turn, these factors were employed in a multi-criteria decision analysis, which hinted for the most suitable crosswind system for an AWE implementation in on-shore rural and off-shore sites - a rigid wing pumping-cycle system with linear horizontal take-off - as well as pointed aerodynamic performance to be the most relevant factor in that decision. Then, this work also presented a framework on the study of high-altitude wind resource in Portugal. The importance of considering atmospheric stability conditions to estimate vertical wind speed and power profiles was acknowledged. Furthermore, for a region of Portugal, it was projected a maximum wind speed of 18 m/s at an altitude of 250 m. This occurred in on-shore areas, which may indicate the exploration of AWE is more advantageous in these type of locations. Finally, a flying testbed to study a future implementation of an AWE *Drag-mode* system was developed. The wind tunnel testing allowed an aerodynamic characterization of the testbed, as well as its power production characteristics. The main conclusions are that with the current electronic setup, the energy production is very inefficient, however, as the flight testing showed, with a power output of 1.3 W at an estimated airspeed of 18.6 m/s, there is potential for future developments.

References

[1] Enerdata. Total primary energy consumption. URL: `https://rb.gy/taiw22`. Visited: 15-03-2022.

[2] H. Ritchie and M. Roser. Energy. URL: `https://rb.gy/xzrx9v`. Visited: 15-03-2022.

[3] Z. Khan and M. Rehan. Harnessing Airborne Wind Energy: Prospects and Challenges. *Journal of Control, Automation and Electrical Systems*, 27:728 – 740, July 2016, DOI: 10.1007/s40313-016-0258-y.

[4] C. L. Archer and K. Caldeira. Global Assessment of High-Altitude Wind Power. *Energies*, 2(2):307–319, 2009, DOI: 10.3390/en20200307.

[5] M. L. Loyd. Crosswind Kite Power. *Journal of Energy*, 4(3), 1980, DOI: 10.2514/3.48021.

[6] Electricity Generation by Energy Sources in Mainland Portugal in 2022. URL: `https://rb.gy/h3iuyc`. Visited: 22-03-2022.

[7] R. Schmehl, U. Ahrens, and M. Diehl. *Airborne Wind Energy*. Green Energy Technology. Springer, 2013. ISBN 978-3-642-39964-0, DOI: 10.1007/978-3-642-39965-7.

[8] R. Schmehl. *Airborne Wind Energy - Advances in Technology Development and Research*. Green Energy Technology. Springer, 2018. ISBN 978-981-10-1947-0, DOI: 10.1007/978-981-10-1947-0.

[9] A. Cherubini, A. Papini, R. Vertechy, and M. Fontana. Airborne Wind Energy Systems: A review of the technologies. *Renewable and Sustainable Energy Reviews*, 51:1461–1476, 2015, DOI: 10.1016/j.rser.2015.07.053.

[10] F. Trevisi. Configuration Optimisation of Kite-Based Wind Turbines. Master's thesis, Technical University of Denmark, Denmark, Oct. 2019.

[11] F. Bauer, R. M. Kennel, C. M. Hackl, F. Campagnolo, M. Patt, and R. Schmehl. Drag Power Kite with Very High Lift Coefficient. *Renewable Energy*, 118:290–305, Apr. 2018, DOI: 10.1016/j.renene.2017.10.073.

[12] T. L. Saaty and L. G. Vargas. *The Analytic Network Process*, pp. 1–26. Springer US, Boston, MA, 2006. ISBN 978-0-387-33987-0, DOI: 10.1007/0-387-33987-6_1.

[13] L. Mikhailov. Deriving priorities from fuzzy pairwise comparison judgements. *Fuzzy Sets and Systems*, 134(3):365–385, Mar. 2003, DOI: 10.1016/S0165-0114(02)00383-4.

[14] A. F. da Cunha Pereira and J. M. M. de Sousa. Assisted site-dependent selection of the most suitable airborne wind energy system via fuzzy analytic network process: Datasets and supplementary materials. URL: `https://data.mendeley.com/datasets/d9xh5552vn/1`.

[15] M. Schelbergen, P. Kalverla, R. Schmehl, and S. Watson. Clustering wind profile shapes to estimate airborne wind energy production. *Wind Energy Science*, 5(3):1097–1120, Aug. 2020, DOI: 10.5194/wes-5-1097-2020.

[16] J. M. M. Sousa. Using Meso-Scale Modelling for the Prediction of Wind Resources in Portugal. In N. H. Afgan and M. G. Carvalho, editors, *New and Renewable Energy Technologies for Sustainable Development*, volume 4 of *5*, chapter Wind Energy Resources, pp. 201–213. Swets & Zeitlinger, 3rd edition, Jan. 2004, DOI: 10.1201/9781003078883-14.

[17] J. B. Barlow, J. William H. Rae, and A. Pope. *Low-Speed Wind Tunnel Testing*. Wiley, USA, 3rd edition, 1999. ISBN 9780471557746.